I&EC research
Industrial & Engineering Chemistry Research

Article

pubs.acs.org/IECR

Fixed Bed Reactor Validation of a Mayenite Based Combined Calcium−Copper Material for Hydrogen Production through Ca−Cu Looping

Alexander Westbye,[†,‡] Asunción Aranda,[†] Gemma Grasa,[§] Pascal D. C. Dietzel,[‡] Luca Di Felice,[*,†] and Isabel Martínez[§]

[†]Department of Environmental Technology, Institute for Energy Technology (IFE), Instituttveien 18, P.O. Box 40, 2007 Kjeller, Norway

[‡]Department of Chemistry, University of Bergen, P.O. Box 7803, Bergen, Norway

[§]Environmental Research Group, Instituto de Carboquímica, Calle Miguel Luesma Castán 4, 50018 Zaragoza, Spain

Supporting Information

ABSTRACT: For the first time, a mayenite based material combining calcium and copper (18.0/37.6/44.4 estimated active wt % CaO/CuO/$Ca_{12}Al_{14}O_{33}$, CuO/CaO = 2.1 [wt/wt]) has been subjected to three full calcium−copper chemical looping combustion (Ca−Cu Looping) cycles in a fixed bed reactor (70.0 g of combined material and 3.5 g of 18.0 wt % Ni/Al_2O_3 reforming catalyst), demonstrating the feasibility of a combined materials approach to hydrogen production through Ca−Cu Looping. Combined materials were characterized by helium pycnometry, mercury intrusion, nitrogen adsorption, X-ray diffraction, thermogravimetric analysis, scanning electron microscopy, and energy dispersive X-ray diffraction before and after reactor testing. A carbon dioxide capture capacity of 14.6−15.0 g CO_2/100 g (640−660 °C, 1.0 MPa, 2.5 kg_{CH_4} kg_{cat}^{-1} h^{-1}), full oxidation, and expected calcination efficiencies (51−64%) were obtained. Combined material performance is comparable to that of segregated materials previously tested in the same experimental rig. Process intensification of Ca−Cu Looping through combined materials development is promising.

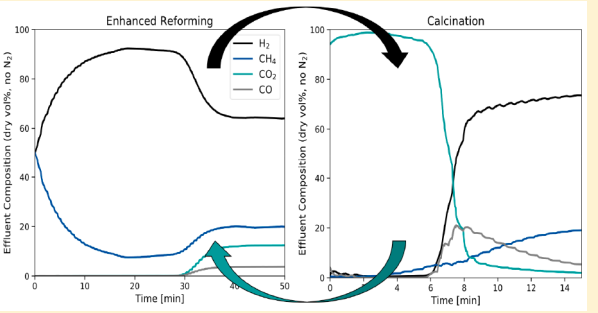

1. INTRODUCTION

Development and implementation of carbon capture and storage technologies (CCS) for mitigation of carbon dioxide (CO_2) emissions has gained traction since the mid-1990s, and it is now generally accepted as an important part of the combination of technologies (alongside renewables, increased energy efficiency, etc.) needed for reaching international emission targets.[1] A 2018 report by the IPCC states with high confidence that it is likely that a 0.8−1.2 °C increase in global average temperature relative to preindustrial levels has already occurred, and an increase to 1.5 °C warming is likely to be reached between 2030 and 2052 if the current rate of CO_2 emission continues.[2] In order to avoid a greater increase of the average temperature, development in both renewable energy technology and CCS is needed.

The primary role of CCS in a future zero/low-emission scenario is anticipated to be captured from stationary fossil fuel based point-sources in power production and the chemical industry.[3] The International Energy Agency (IEA) has underlined the importance of new CCS technologies and the funding of major CCS pilot projects, as large-scale demonstration of CO_2 capture technology is a current bottleneck for more widespread implementation and acceptance in the industrial sector.[4]

The topic of the presented work is hydrogen production from natural gas with CCS, i.e., CO_2 capture from a stationary point-source within the chemical industry. The annual global production of hydrogen is approximately 65 Mt/year where 95% is produced from fossil fuels (48% from reforming of natural gas) and the majority of hydrogen is "used where it's produced" in refinery feedstock hydrotreatment or in the production of miscellaneous commodity chemicals (ammonia, methanol, etc.).[5,6] The associated CO_2 emissions for a large-scale, hydrogen producing natural gas reforming plant are estimated to be in the order of 7.0−8.1 tCO_2/tH_2.[7,8] As an important side note it should be mentioned that there is political interest and drive toward prioritizing CCS technology in these sectors. In, e.g., Norway, ammonia, methanol, and cement production are important constituents of the industrial

Received: April 30, 2019
Revised: July 12, 2019
Accepted: July 15, 2019
Published: July 15, 2019

DOI: 10.1021/acs.iecr.9b02372
Ind. Eng. Chem. Res. XXXX, XXX, XXX−XXX

output,[9,10] and there are possibilities for off-shore CO_2 storage,[11] making CCS an attractive mitigation option.

An emerging technology for hydrogen production with carbon capture is calcium−copper chemical looping combustion (Ca−Cu Looping), where calcium looping (CaL)[3] and chemical looping combustion (CLC)[12,13] are combined into a unified approach for hydrogen production with integrated carbon capture using natural gas or other carbonaceous, gaseous fuels (e.g., biogas). The development of the processing concept can be traced back to ideas of unmixed combustion[14] elaborated by the research group of Abanades et al.[15,16] and developed into a five-step parallel fixed bed reactor concept for hydrogen production.[17] Ca−Cu Looping can also be used for power generation,[18,19] and it has favorable properties for integration with an ammonia plant as both pressurized hydrogen and nitrogen are available in the process.[20]

In conventional steam methane reforming (SMR), steam and light hydrocarbons (e.g., methane, CH_4) are fed into tubular reformers (FTRs) where the water−gas-shift (WGS) and reforming reactions[21,22] take place over a catalytic bed of solids, often using a nickel-based catalyst.[23−25] Effluent temperatures and pressures are in the order of 850−900 °C and 2.5 MPa. The energy required for the net endothermic reforming reaction system is provided by the combustion of fuel gas.[26] From a thermodynamic point of view, low operating pressure and high temperature are favorable, but an economic incentive exists for high pressure operation in spite of increased methane slip as this enables process intensification.[27] For hydrogen production through conventional reforming, shift reactor(s) are required to drive the WGS reaction in the direction of hydrogen, and a separation of a gaseous CO_2/H_2 mixture is required downstream.

The first of three main steps in Ca−Cu Looping utilizes the concept of sorption enhanced reforming (SER).[28,29] In SER, a calcium oxide (CaO) based CO_2 sorbent is introduced into the reforming reaction system alongside the reforming catalyst. As CO_2 is generated from the reforming reaction system, calcium carbonate ($CaCO_3$) is formed by the carbonation of CaO in an exothermic reaction ($\Delta_r H°(298\ K) = -178.8\ kJ\ mol^{-1}$). The heat from carbonation provides the energy necessary for reforming while also removing the requirement for fuel gas burning outside the tubular reactors. The equilibrium production of hydrogen shifts toward 90−95 vol % (dry) depending on pressure, sorbent content, feed composition, and temperature conditions. Typically, SER in a fixed bed reactor is performed at 650−700 °C and 0.1−2 MPa with molar steam-to-carbon ratios (S/C) of 2.5−5.0 and a methane mass hourly space velocity ($MHSV_{CH_4}$) ≥ 0.75 $kg_{CH_4}\ kg_{cat}^{-1}\ h^{-1}$.[17] Some advantages of SER relative to SMR are higher hydrogen purity, no shift reactor requirement, lower operating temperature, no fuel gas burning, and CO_2/H_2 separation being inherent to the process.

The major challenge related to SER is the energy intensive regeneration of the CaO sorbent from $CaCO_3$ (calcination), where the sorbent must be calcined in a high percentage CO_2 environment at high temperature ($P^{eq.}_{CO_2}$ = 0.1 MPa at 898 °C[30]). In Ca−Cu Looping, the proposed solution to the CaO regeneration challenge is a coupling of sorbent regeneration and the redox reaction system of elemental copper and copper(II) oxide (Cu/CuO). The second step in Ca−Cu Looping is thus exothermic oxidation of elemental copper to copper(II) oxide in an air reactor operated at 300−800 °C and 1−2 MPa in oxygen diluted air (e.g., 2.5−5 vol % O_2).

In the third processing step (calcination step), H_2 provided from hydrogen-rich adsorber off-gas and CH_4/CO available elsewhere in the process (e.g., fuel feedstock or reforming) are used to drive exothermic reduction of CuO and generate the heat necessary for CaO regeneration. The output from this step will in theory be a CO_2/H_2O gas mixture from which CO_2 can easily be separated and stored.

The energy balance in the calcination step is in large determined by the copper-to-calcium ratio (CuO/CaO). In general, the determination of an appropriate CuO/CaO is not trivial as it depends on the initial reactor temperature (i.e., process heat integration), reducing gas composition, flow conditions, the degree of $CaCO_3$ loss during oxidation, the degree of carbonation in the SER step, etc. CuO/CaO weight ratios between 2.4 and 3.1 [wt/wt] (CuO/CaO 1.7−2.2 [mol/mol]) have been reported as optimal based on thermodynamic and process modeling for a representative $CH_4/CO/H_2$ reducing gas,[17,31−33] while using CH_4 only as a reducing gas will require CuO/CaO weight ratios of about 4.5 (3.2 molar).[34]

A 2018 techno-economic assessment of Ca−Cu Looping integrated in a hydrogen plant by Riva et al.[7] shows that Ca−Cu Looping compares favorably to a base-case FTR w/amine capture. Capital cost is a significant contributor to the total economic potential of the Ca−Cu Looping concept, and further process intensification through, e.g., materials development for Ca−Cu Looping, could contribute to driving down cost. One method for intensifying the process is demonstrated in this work through a two-particle approach (or "combined materials approach")[35−38] to Ca−Cu Looping, in contrast to the commonly implemented three-particle approach (or "segregated materials approach"). In the combined materials approach, CuO and CaO phases are integrated into one particle. Given segregated particles with active weight loadings of 30 wt % CaO and 70 wt % CuO, a 40 wt % CuO loaded combined material would give more active material per gram for the recommended 2.4−3.1 [wt/wt] (1.7−2.2 [mol/mol]) CuO/CaO ratio range. The hypothesized advantages of this approach relative to the segregated approach in addition to process intensification include better heat transfer properties and avoiding hot spots due to the intimate contact between Ca and Cu species during calcination as well as two rather than three materials production lines. However, segregated and combined materials face the same major challenge: stable transient CO_2 and O_2 carrying capacities across a sufficient number of process cycles complicated by CaO sintering and CuO migration.

In a previous study, our research group at IFE evaluated the performance of combined materials based on mayenite ($Ca_{12}Al_{14}O_{33}$) at CuO/CaO = 2.0 [wt/wt] (1.41 [mol/mol]) and CuO loadings of 40 and 50 wt % using various CuO precursors in a hydrothermal synthesis.[39] It was shown that materials at 50 wt % CuO loading deactivated regardless of precursor during Ca−Cu Looping relevant cyclic thermogravimetric analysis (TGA, 40 cycles), while 40 wt % CuO loaded materials remained active. The CuO/CaO = 2.0 [wt/wt] ratio was chosen as it (1) represents a maximum expected CaO content for a given CuO loading, (2) if a material is stable at CuO/CaO = 2.0 [wt/wt] at a given CuO loading, it should be stable at higher CuO/CaO ratios at the same CuO loading (increasing the CuO/CaO ratio is equivalent to replacing a

DOI: 10.1021/acs.iecr.9b02372
Ind. Eng. Chem. Res. XXXX, XXX, XXX−XXX

CaO phase that is potentially sintering with a highly stable calcium aluminate phase), and (3) CaO has a well-established carbonation behavior that is dominated by a kinetic- and a diffusion-controlled regime. It is likely that the CO_2 carrying capacity of the CaO sorbent cannot be fully utilized under all operating conditions and process configurations due to mass transfer limitations.[40] In 0.1 MPa TGA tests the kinetic regime carbonation of CaO represented 75−80% of the total CaO conversion, giving active CuO/CaO ratios of 2.5−2.7 [wt/wt] (1.8−1.9 [mol/mol]) if only the kinetic carbonation regime could be utilized in practical application. Copper oxidation is fast and is assumed to be complete based on studies of copper based oxygen carriers.[41] The material used for the present validation is a 40 wt % CuO loaded $CaO/CuO/Ca_{12}Al_{14}O_{33}$ material prepared using $Cu(OH)_2$ with a CuO/CaO = 2.0 [wt/wt].

Previous investigations into larger scale Ca−Cu Looping have been performed with an emphasis on a three-particle system approach where catalyst particles, a CaO based sorbent, and a Cu based oxygen carrier have been used in a fixed bed under relevant conditions. A validation of the SER step was performed by Grasa et al.[42] using 3.2−4.0 molar *S*/*C*, sorbent-to-catalyst ratio (*Z*) of 4−15, and 0.1−0.9 MPa pressure, where a $MHSV_{CH_4}$ = 2.5 h^{-1} was found suitable for a mayenite based sorbent ($CaO/Ca_{12}Al_{14}O_{33}$). Fernández et al.[43] have recently demonstrated calcination in pure methane at TRL 4, using a 60 wt % Cu/SiO_2 commercial oxygen carrier and commercial CaO sorbent. Of special interest is the work of Díez-Martín et al.[44] where a complete cyclic Ca−Cu Looping process was demonstrated under relevant conditions using a mayenite based sorbent (39.0 g CO_2/100 g initial capacity, 20.0 g CO_2/100 g residual capacity), a 65 wt % Cu oxygen carrier, and an 18 wt % Ni/Al_2O_3 catalyst. In terms of combined materials testing, a preliminary study of SER conditions using a 22/53/25 wt % $CaO/CuO/Ca_{12}A_{l4}O_{33}$ combined material[45] has been performed with results comparable to those of Díez-Martín et al. using the same fixed bed reactor.[46]

In this work, the approach that Díez-Martín et al. used to test segregated materials is followed closely in a first validation of the combined material approach using full Ca−Cu Looping cycles in a fixed bed reactor. The purpose of the presented experiment is validation and critical evaluation of laboratory scale estimations and assumptions by exposing material agglomerates to realistic SER, oxidation, and calcination conditions at elevated pressure at 70.0 g scale. The focal points are the characterization and cyclic behavior of a 40 wt % CuO loaded $CaO/CuO/Ca_{12}Al_{14}O_{33}$ combined material prepared using $Cu(OH)_2$ as copper(II) oxide precursor in a hydrothermal synthesis. This material represents a potentially low-cost combined material that could provide the best material configuration for Ca−Cu Looping in terms of process intensification. Reactor tests and characterization have also been performed on a 40 wt % CuO loaded $CaO/CuO/Ca_{12}Al_{14}O_{33}$ combined material prepared using CuO powder as copper(II) oxide precursor in order to illustrate reproducibility of results, as results for these two materials are expected to be comparable.[39]

2. MATERIALS AND EXPERIMENTAL METHOD

2.1. Preparation of Material. The combined calcium−copper material was prepared using a hydrothermal synthesis route previously reported by our group,[39] where 3.0 g powder batches of combined calcium−copper materials were studied in detail using various CuO loadings and precursors. A theoretical calcined combined material composition of 20/40/40 wt % $CaO/CuO/Ca_{12}Al_{14}O_{33}$ with an active CuO/CaO = 2.0 [wt/wt] ratio using $Cu(OH)_2$ as CuO precursor was selected for upscaling based on favorable results and precursor cost. Synthesis scale-up to 100.0 g batches, as well as an agglomeration procedure, has been reported.[47] The essential features of materials synthesis and agglomeration of the tested material are summarized here for ease of reference.

For the upscaled synthesis of combined calcium−copper mayenite based material, copper hydroxide ($Cu(OH)_2$, technical grade, Sigma-Aldrich), boehmite (AlO(OH), 95% Sasol), and calcium hydroxide ($Ca(OH)_2$, >99% Merck) were used as reactants, and isopropyl alcohol and deionized water were used as solvents. Dried reactants (>48 h, 110 °C) corresponding to a theoretical 40 wt % CuO loaded combined material with CuO/CaO = 2.0 [wt/wt] were weighed out and mixed in isopropyl alcohol with a solid-to-liquid ratio of 4.0. The slurry was stirred for 1 h at room temperature, dried overnight in a 110 °C laboratory oven, mixed with deionized water using a solid-to-liquid ratio of 3.0, transferred to a 600 cm^3 stainless steel autoclave, and heated to 150 °C (2 °C min^{-1} heating rate) resulting in an absolute pressure of 0.5 MPa inside the autoclave. The liquid−solid mixture was kept at these conditions for 5 h and subsequently cooled to ambient temperature (2 °C min^{-1} cooling rate). A laboratory oven was used in order to evaporate the solvent overnight (110 °C, 16 h). The resulting dried solid was crushed to a fine powder and calcined at 1000 °C (1 h, 5 °C min^{-1} heating rate). A yield of 95−97 wt % can be expected from the described procedure using a theoretical 100.0 g of oxidized and calcined solids production as basis.

Agglomeration through wet granulation is scalable and frequently employed in industry. Calcined powders were agglomerated in a GMX-LAB Micro High Shear Wet Granulator (Vector Corporation). Batches of 95.0 g of material were agglomerated using a 1.0 L agglomeration bowl, 500 rpm impeller, and 500 rpm chopper speed. An aqueous solution of 15 wt % polyethylene glycol (PEG) was used as a binder and added to the solids with a 10 rpm pump speed. 40.0 g of PEG was used per 100.0 g of powder. Sieving after agglomeration resulted in a 35−40 wt % yield in the agglomerate diameter range of 0.5−0.8 mm. This size fraction was selected for reactor testing. Agglomerates were calcined at 900 °C (1 h, 5 °C min^{-1} heating rate) in order to remove the PEG binder.

The same synthesis and agglomeration procedure was used for the combined material presented in the Supporting Information (Figures S4−S12, Tables S1−S3) using CuO powder (>97 wt % 325 Mesh Powder, Alfa Aesar) as copper(II) oxide precursor.

2.2. Material Characterization. Prepared agglomerates were characterized before and after fixed bed reactor testing. Characterization before testing included cyclic thermogravimetric analysis (TGA) representing process relevant Ca−Cu Looping conditions (section 2.3), X-ray diffraction (XRD), helium (He) pycnometry, mercury (Hg) intrusion, N_2 adsorption, scanning electron microscopy (SEM), and energy dispersive X-ray spectroscopy (EDX). After reactor testing the same characterization methods except TGA cycling were used. All characterization before and after testing was performed with materials in a calcined and oxidized state. After reactor

DOI: 10.1021/acs.iecr.9b02372
Ind. Eng. Chem. Res. XXXX, XXX, XXX−XXX

Table 1. Normal Gas Flow (101.325 kPa, 273.15 K), Set Point Temperature, and Pressure for the Ca−Cu Looping Reactor Tests for 70.0 g of Combined Material (15.0 wt % Active CaO) and 3.5 g Reduced 18.0 wt % Ni/Al_2O_3 Catalyst[a]

	pressurization	SER	flush	acc 1	oxidation	acc 2	calcination
	800 to 625 °C	625 °C	625 to 700 °C	700 °C	700 °C	700 to 800 °C	800 °C
	0.1 to 1.0 MPa	1.0 MPa	1.0 MPa	1.0 to 0.8 MPa	0.8 MPa	0.8 to 0.1 MPa	0.1 MPa
	15 min	60 min	15 min	30 min	65 min	15 min	20 min
N_2 [NL/h]	46.3	2.7	46.3	36.0	28.8	30.9	2.7
H_2 [NL/h]	5.1		5.1				25.7
H_2O [NL/h]		38.7					
CO_2 [NL/h]				15.4	19.0	20.5	
CH_4 [NL/h]		12.3					10.5
O_2 [NL/h]					3.6		
total [NL/h]	51.4	53.7	51.4	51.4	51.4	51.4	39.0

[a]Molar S/C = 3.15, sorbent-to-catalyst mass ratio (Z) = 3.0, $MHSV_{CH_4}$ = 2.5 h^{-1}. Acc = accommodation step.

testing, the materials were treated in air at 600 °C for 1 h in order to oxidize the postcalcination elemental copper.

XRD data was collected using a Bruker D8 Advance diffractometer with a monochromatic CuK_α source and operating at 40 kV and 40 mA. An instrument alignment accuracy of 0.01° according to the UNE-EN-13925 standard was implemented.

True density was determined using a Micromeritics AccuPic II for He pycnometry, a method based on the displacement of a known volume of He by the solid materials. Results for true density can be obtained with an accuracy of 0.03%.

Hg intrusion was performed in a Micromeritics AutoPore V instrument in accordance with the ISO 15901 norm in order to determine particle porosity through pore structure and distribution. The accuracy of the instrument is determined to 0.04 mL of Hg.

N_2 adsorption at 77.0 K was performed using a Micromeritics ASAP 2020 instrument according to the ISO 9277 standard. Physisorption data was interpreted using the Brunauer−Emmett−Teller (BET) model. Relative pressures (P/P_0) up to 0.3 were used. Instrument accuracy can be taken as 0.02 m^2 g^{-1}.

A Hitachi S-3400 N was used for SEM/EDX measurements in order to evaluate particle morphology and elemental distribution in the solid samples. Surface images, cross-sectional images and elemental mapping is reported in this work.

2.3. Experimental TGA Setup and Testing Conditions.

Samples from as-prepared upscaled powder and agglomerates were subjected to cyclic, process relevant Ca−Cu Looping TGA tests in order to evaluate transient stability across cycles and for estimation of CO_2 and O_2 carrying capacities. Results were used for quality control of upscaled powder and agglomerates and for establishing fixed bed reactor flow conditions through estimation of the maximum expected active CaO wt % content in the combined material. The gas composition, temperature, and time-on-stream for all steps in the Ca−Cu Looping TGA cycles are described in detail in previous work.[39] In brief, the TGA apparatus consists of a cylindrical alumina (Al_2O_3) tube (height: 80.0 cm, thickness: 4.0 mm, internal diameter: 3.5 cm) embedded in a furnace. A porous alumina crucible (thickness: 1.0 mm, height: 16.0 mm, external diameter: 7.0 mm) is used as sample holder. The total gas flow is 500 mL(STP) min^{-1}, and H_2 (6.0, Praxair), N_2 (5.0, Praxair), CO_2 (5.0, Praxair), synthetic air (21% O_2, 79% N_2, 6.0, Praxair), and steam (H_2O(g), deionized) can be utilized. The vessel can operate at ambient pressure and between ambient temperature and 900 °C at a heating and cooling rate of 9 °C min^{-1} and 3.5 °C min^{-1}, respectively.

In a typical test, 25.0 mg was taken from a well-mixed sample container of either agglomerates or finely crushed powder. Samples were placed in the calibrated alumina crucible and heated to 870 °C in 400 mL(STP) min^{-1} synthetic air and 100 mL(STP) min^{-1} N_2. After an initial N_2 flush and a reduction/calcination step at 870 °C, cycles representing realistic Ca−Cu Looping conditions at ambient pressure were performed−carbonation with steam (650 °C), oxidation (650 °C), reduction (875 °C), and calcination (875 °C). All samples were cooled to ambient temperature in 500 mL(STP) min^{-1} synthetic air after the last calcination/reduction step. 40 TGA cycles were performed for the reported samples at 159 min per Ca−Cu Looping cycle (5.52 days of continuous TGA testing).

Capacity data reported from TGA tests are given in g/100 g with respect to 100.0 g of a calcined and reduced combined mayenite material ($CaO/Cu/Ca_{12}Al_{14}O_{33}$), while all compositional estimates are given on an oxidized and calcined basis ($CaO/CuO/Ca_{12}Al_{14}O_{33}$).

2.4. Experimental Reactor Setup and Operating Conditions.

A schematic and thorough description of the fixed bed reactor used in this experimental work can be found in Díez-Martín et al.[44] which serves as the foundation for the described reactor tests. The tubular reactor is a quartz wool isolated, vertical stainless-steel vessel (internal diameter: 18.0 mm, bed length: 0.2 m, capacity: 90.0 g) heated with a 5.0 m 1.25 kW heating wire. The reactor has an overall heat transfer coefficient of 9.5 W m^{-2} K^{-1} given an ambient temperature of 25 °C and a reactor temperature of 900 °C at 0.1 MPa. The vessel is equipped with 15 thermocouples (TCs) placed vertically along the reactor bed spaced in 2.5 cm intervals. A control TC is placed just above the porous plate that contains the agglomerates. Inlet gas (H_2, H_2O, CO, CO_2, CH_4, N_2, and O_2) is preheated to 400 °C. Temperature data is collected instantaneously, while the reactor effluent is analyzed using a gas analyzer for dry gas composition (N_2 and O_2 are not directly measured). The reactor was operated at temperatures and pressure up to 875 °C (20 °C min^{-1} heating rate) and 1.0 MPa. A pressure-drop over the reactor bed in the order of 10 kPa was registered during all stages of testing. Gas compositions for all the steps in the testing regime are summarized in Table 1. Three cycles were performed for the presented material. Nitrogen (Table 1) was introduced as an inert gas in order to calculate the total dry flow out of the reactor.

DOI: 10.1021/acs.iecr.9b02372
Ind. Eng. Chem. Res. XXXX, XXX, XXX−XXX

Materials (70.0 g CaO/CuO/$Ca_{12}Al_{14}O_{33}$ and 3.7 g oxidized 18.0 wt % Ni/Al_2O_3 catalyst) were top loaded into the vertical reactor bed giving a height of about 13.1 cm. The TC placements were thus at 2.5 cm (TC5), 5.0 cm (TC4), 7.5 cm (TC3), 10.0 cm (TC2), and 12.5 cm (TC1) measured from the bed bottom. The upper part of the solids bed, between 12.5 and 13.1 cm, was not covered by thermocouples. 15.0 wt % active CaO was assumed for the combined material—a reasonable estimate between powder and agglomerate capacities from TGA tests (Table 2).

Table 2. Characterization Data for Powder and Agglomerates (0.5−0.8 mm) before Reactor Testing[a]

	powder	agglomerates
surface area [m^2 g^{-1}]		2.19 ± 0.01
true density [g cm^{-3}]		3.67 ± 0.01
average pore diameter [nm]		381.4
porosity [%]		53.6
particle density [g cm^{-3}]		1.70
TGA (g CO_2/100 g)$_{max}$	15.3	11.6
TGA (g O_2/100 g)$_{max}$	8.2	6.0
TGA wt % CaO	18.0	13.9
TGA wt % CuO	37.6	28.1
TGA CuO/CaO [wt/wt]	2.1	2.0

[a]True density is based on He pycnometry. Porosity, average pore diameter, and particle density are based on Hg intrusion, while surface area is based on N_2 adsorption (BET).

Prior to initiating the Ca−Cu Looping cycle, a prereduction using the pressurization step gas composition (Table 1) was performed, making sure that the catalyst and combined material were in reduced and calcined states. Materials were heated in N_2 and H_2 to form ambient temperature to 800−850 °C and kept at these conditions until no CO_2 was detected by the gas analyzer and no H_2 was consumed. After this prereduction step, the material was cooled, and the full pressurization conditions (0.1 to 1.0 MPa at 625 °C set point temperature) were imposed and kept for 15 min for conditions to stabilize. When conditions were stable, steps according to Table 1 were performed, representing a full cycle of Ca−Cu Looping. After the calcination step, the materials were cooled at ambient pressure using the pressurization step gas composition (Table 1). Prereduction was performed prior to each reported cycle.

Testing conditions reported in Table 1 were selected based on previous work on segregated materials reactor experimentation[44] and reported optimal operation conditions for Ca−Cu Looping.[17] The SER step was performed using a molar *S*/*C* of 3.15, 0.97−1.0 MPa pressure, and set point temperature of 625 °C. These conditions are suitable for high CH_4 conversion at elevated pressure and for avoiding significant CaO hydration. A temperature of 625 °C refers to the reactor set point temperature, and a temperature gradient of 20 °C was observed between the top and bottom TCs during testing. A set point of 625 °C corresponds to initial bed temperatures between 640 and 660 °C. A sorbent-to-catalyst mass ratio (*Z*) of 3.0 was selected, defined as "mass of active CaO to reduced catalyst particle", where the catalyst particle is a 15.9−20 wt % Ni Johnson Matthey HiFUEL R110 commercial catalyst described elsewhere[48] and referred to as a 18.0 wt % Ni/Al_2O_3 material in this work. A $MHSV_{CH_4}$ of 2.5 h^{-1} (>0.75 h^{-1}) was selected for the SER step based on previous testing of a combined 22/53/25 wt % CaO/CuO/$Ca_{12}Al_{14}O_{33}$ material.[46]

Oxidation conditions were fixed at 0.8 MPa pressure, a 700 °C temperature set point, and 7.0 vol % O_2 representing diluted air. Several reactors are not operated in parallel in this work. Heat exchange and recarbonation after oxidation is thus not possible. Copper oxidation causes an elevation in temperature, and in combination with a CO_2 partial pressure close to zero, calcination will occur. To counter this effect, 37.0 vol % CO_2 was sent in together with N_2 and O_2. The slight increment in O_2 volume fraction from 2.5−5.0 vol % to 7.0 vol % was merely a practical consideration in order to keep the flow for each step fairly similar and at the same time allow for oxidation in a reasonable time frame. It will be shown in section 3.2 that this is an appropriate choice.

The calcination step was performed at 0.1 MPa with an 800 °C set point temperature and a reducing gas composition of 27 vol % CH_4 and 66 vol % H_2 (balance N_2). With the employed gas composition, 62−81% of the energy required for $CaCO_3$ calcination is expected from CuO reduction alone, depending on the active weight fraction of CaO. For reference, this value would be 89.2% with a CuO/CaO = 2.8 [wt/wt] and a gas composition of 27.0 vol % CH_4, 54.0 vol % H_2, and 12.0 vol % CO feed composition, i.e., reported optimal conditions for upscaled operation. Although full sorbent regeneration is not expected, the incorporated cooling procedure and precalcination (800−850 °C, 0.1 MPa) provide full calcination/reduction of the material prior to subsequent Ca−Cu Looping cycling. Future work must be dedicated to fine-tuning of inlet gas composition, flow rate, bed initial temperature, and material composition in order to optimize calcination efficiency, as this is outside the scope of the presented work.

3. RESULTS AND DISCUSSION

3.1. Material Characterization before Reactor Testing. The X-ray diffraction pattern of prepared agglomerates prior to reactor testing is presented in Figure 1. All diffraction peaks have been accounted for and identified as $Ca_{12}Al_{14}O_{33}$, CuO, Ca_2CuO_3, and $CaCu_2O_3$. The presence of mixed calcium−copper phases was expected based on observations

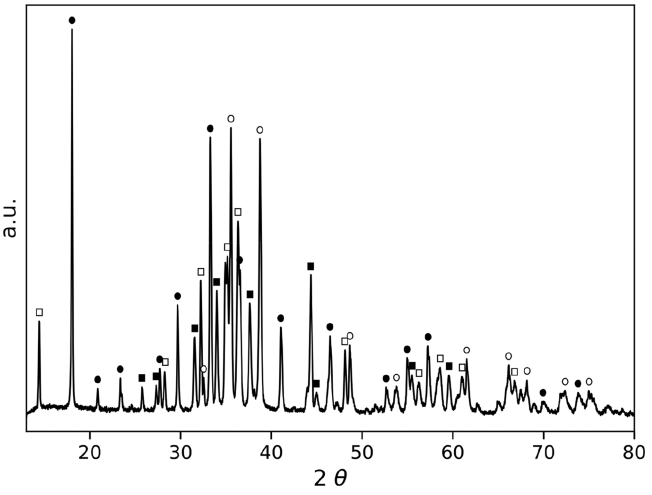

Figure 1. Diffraction pattern for calcined (1 h, 900 °C) 0.5−0.8 mm agglomerates before reactor testing. All peaks are accounted for and identified as CuO (○), $Ca_{12}Al_{14}O_{33}$ (●), Ca_2CuO_3 (□), and $CaCu_2O_3$ (■).

DOI: 10.1021/acs.iecr.9b02372
Ind. Eng. Chem. Res. XXXX, XXX, XXX−XXX

made previously for combined material powders prepared using $Cu(OH)_2$.[39] 3.0 g of laboratory scale powders was almost exclusively composed of mayenite and mixed phases (e.g., 48.3 wt % $CaCu_2O_3$, 15.6 wt % Ca_2CuO_3, and 0.8 wt % CuO at 20/40/40 wt % $CaO/CuO/Ca_{12}Al_{14}O_{33}$),[39] while it seems to be a more pronounced contribution from CuO to the agglomerate spectrum. This can be an indication of a less ideal mixing during upscaling, as mixed phases are likely related to intimate contact between Ca and Cu species during hydrothermal synthesis prior to calcination in air (1000 °C).

Characterization data for the as-synthesized upscaled powder and 0.5−0.8 mm diameter agglomerates are summarized in Table 2. Transient TGA behavior during 40 Ca−Cu Looping relevant cycles is presented graphically in Figure 2. Particle surface area was determined using N_2 adsorption and the theoretical framework of Brunauer−Emmett−Teller (BET). The characterization data in Table 2 show that the agglomerates have high porosity and relatively low surface area. The characterization data reported are all within an expected range of values for combined calcium−copper materials.

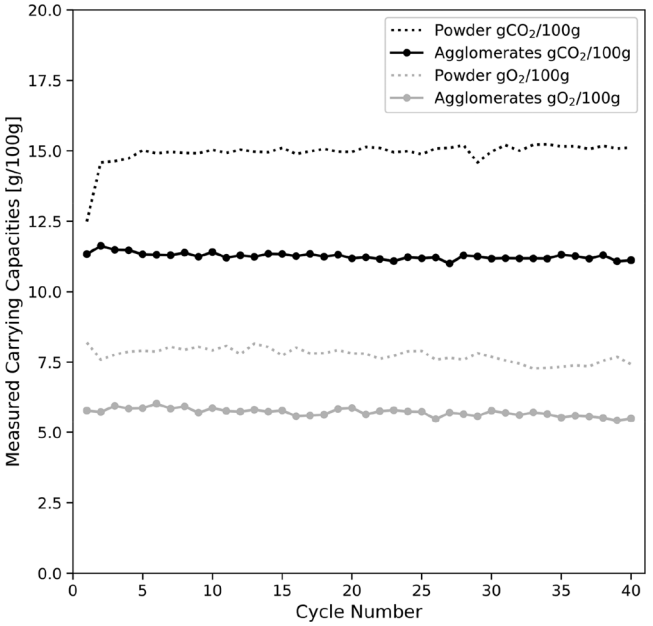

Figure 2. Measured g CO_2/100 g and g O_2/100 g carrying capacities for the investigated powder and agglomerates. Carrying capacities are reported using g/100 g calcined and reduced combined material as basis ($CaO/Cu/Ca_{12}Al_{14}O_{33}$). Adapted with permission from ref 47. Copyright 2019.

Satisfactory stability across 40 TGA cycles is observed for both powder and agglomerates. Maximum capacities of 15.3 g CO_2/100 g and 8.2 g O_2/100 g were registered for the powder, equivalent to a 18.0/37.6/44.4 wt % $CaO/CuO/Ca_{12}Al_{14}O_{33}$ material with respect to active phases and an active CuO/CaO = 2.1 [wt/wt]. It has been shown in previous work that compositional estimates based on maximum registered TGA capacities and Rietveld refinement are in good agreement for the material in question.[39] The TGA estimate can be taken as an accurate lower estimate of true (active phase + inactive or inaccessible phase) CuO and CaO loading.

There is a 26.8 wt % drop in g O_2/100 g and 24.2 wt % drop in g CO_2/100 g carrying capacity in the agglomerates relative to the powder given the same testing conditions and time duration for carbonation and oxidation in the TGA. Given the similarities in powder and particle phase composition before testing and the similar weight-based reduction in O_2 and CO_2 capacities both, the difference between powder and agglomerate capacities is attributed to mass transfer limitations. It can be expected that the actual active phase material composition during the reactor test will be between 13.9/28.1/58.0 and 18.0/37.6/44.4 wt % active $CaO/CuO/Ca_{12}Al_{14}O_{44}$ depending on the extent of mass transfer resistance during the SER and oxidation steps.

In Figure 3(a), the SEM of the agglomerate surface indicates a good dispersion of copper (light gray) and a $CaO/Ca_{12}Al_{14}O_{33}$ phase (dark gray). An EDX mapping along with a SEM image is provided in Figure 3(b)−(e). A slight tendency toward Cu clustering can be observed in (b); however, the dispersion of elements on the particle level is homogeneous with an abundance of Ca and Al relative to Cu, as expected due to the Ca and Al rich mayenite support structure.

A 40 wt % CuO loaded combined material prepared using CuO powder has also been characterized using the same techniques (Supporting Information, Figures S4−S12, Tables S1−S3). The characterization data are comparable. The CuO prepared material has more pronounced CuO clustering and indications of a lower mass transfer resistance in agglomerate TGA performance relative to that of powder. This is consistent with previous observations.[39]

3.2. Ca−Cu Looping Tests in a Fixed Bed Reactor.

3.2.1. Sorption Enhanced Reforming (SER). Figure 4 depicts measurements of dry volume percent (vol %) composition in the reactor effluent and thermocouple temperatures as functions of time during the SER step at 0.97−1.0 MPa, S/C = 3.15, $MHSV_{CH_4}$ = 2.5 h^{-1}, Z = 3.0, and 640−660 °C initial bed temperatures. A plot of temperature profiles in Celsius can be found in the Supporting Information (Figure S1).

In Figure 4 (*left*), following the introduction of reactants, the measured vol % of CH_4 and H_2 go through a 10−15 min transient period (the smooth profile and differences in initial and breakthrough H_2 slopes must be seen in relation to a combination of flow dispersion in the condenser, low superficial velocity, and initial transient instabilities in CH_4 and steam feed) until conditions close to expected SER equilibrium are established in all three cycles (92.7 vol % H_2 dry at S/C = 3.15, P = 0.97 MPa at T = 660 °C). The maximum dry vol % H_2 registered in the reactor effluent for the three cycles was 91.5, 92.3, and 91.0 vol %, corresponding to 98.7%, 99.6%, and 98.2% of the calculated SER equilibrium values. Thus, ≥98.2% [vol/vol] of the calculated SER H_2 equilibrium value was obtained during testing for all three cycles.

After 10 min at a plateau close to SER equilibrium conditions, the active calcium oxide was carbonated, and a well-defined breakthrough occurred during a 5 min window. The breakthrough is sharp and does not show any significant signs characteristic to that of diffusion regime carbonation. The breakthrough was followed by establishment of SMR equilibrium (63.8 vol % H_2 dry at S/C = 3.2, P = 0.985 MPa, and T = 640 °C). A carbon balance over the SER step results in calculated active CaO loadings ($CaO/CuO/Ca_{12}Al_{14}O_{33}$ basis) of 17.2 wt % (14.6 g CO_2/100 g) for the first, 17.7 wt % (15.0 g CO_2/100 g) for the second, and 17.5

DOI: 10.1021/acs.iecr.9b02372
Ind. Eng. Chem. Res. XXXX, XXX, XXX−XXX

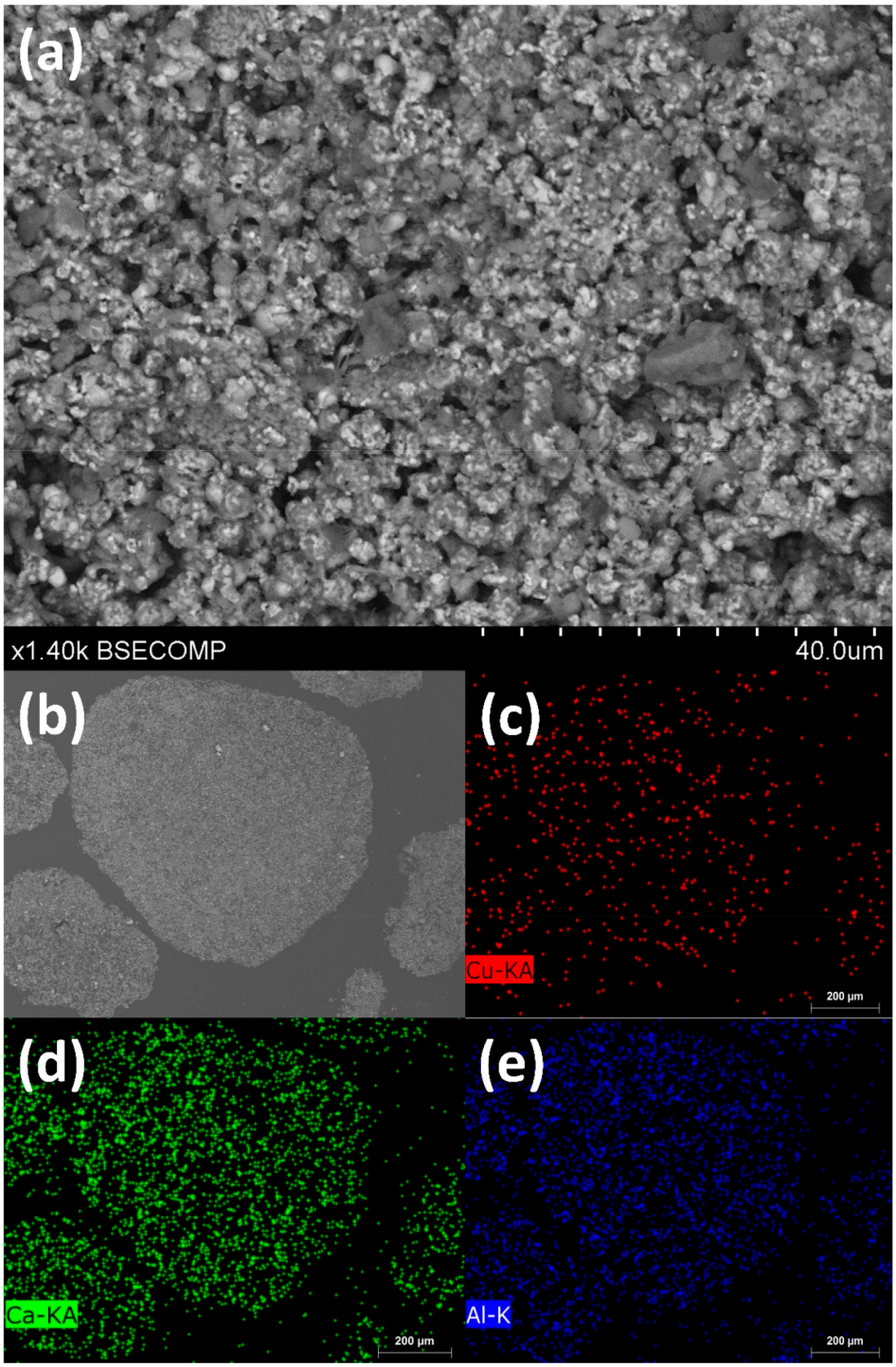

Figure 3. (a) SEM of the particle surface. (b)−(e) Cross-sectional SEM image and EDX mapping of the agglomerate before reactor testing. Cu, Ca, and Al show an even dispersion throughout the agglomerate sample with slight indications of Cu clustering (light gray) areas in (b).

wt % (14.8 g CO_2/100 g) for the third cycle. This corresponds to 95.4%, 98.0%, and 96.7% carbonation of the estimated active CO_2 carrying capacity of the TGA tested powder. Based on these values it seems evident that the mass transfer limitations observed in the TGA (Figure 2) for the agglomerates relative to powder are not present at higher pressure using the stated operating conditions. Previous works have reported lower sorption capacity in packed beds as compared to TGA under atmospheric pressure, ascribable to a convective transport through the bed and toward the reactor exit which makes complete CaO conversion less favorable.[49−51] In this work, the pressurized condition resulted in 1) high contact time, 2) improved driving force for CO_2 transport through the boundary layer and into the particle—resulting in an increased transfer rate, and 3) as an effect of Le Châtelier's principle, a shift in the equilibrium toward CO_2 capture—the side of the reaction with lesser gaseous moles—to counterbalance the pressure increase. These factors contribute in making the as-prepared powder CO_2 capture estimate from

DOI: 10.1021/acs.iecr.9b02372
Ind. Eng. Chem. Res. XXXX, XXX, XXX−XXX

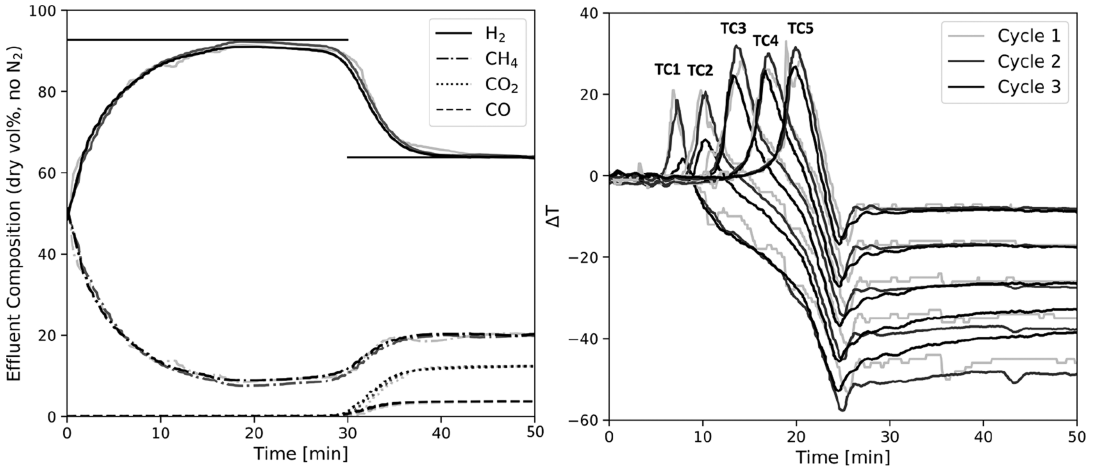

Figure 4. Dry volume percentage measurements (*left*) and thermocouple (TC) temperature difference ΔT [°C] (*right*) as functions of time during the Ca−Cu Looping SER step for the described combined calcium−copper material (0.97−1.0 MPa, 640−660 °C initial temperature, S/C = 3.15, Z = 3.0, $MHSV_{CH_4}$ = 2.5 h^{-1}). Solid lines (*left*) illustrate SER and SMR equilibrium (dry) vol % H_2 at the given conditions.

the 0.1 MPa TGA test representative of high-pressure sorbent function performance.

Considering Figure 4 (*right*), the characteristic heat evolution expected for fixed bed SER operation is clearly observed. A hot front moves down the vertical reactor, evident through the transient development of temperature profiles for the TC1−TC5 thermocouples, TC1 being placed 12.5 cm into the 13.1 cm bed of material, closest to the reactor inlet. Using TC1 in the second cycle as an example, a sharp rise in temperature occurs when CO_2 from the SMR reaction system carbonates CaO. The TC1 temperature reaches a peak value followed by a decline. At this point the active sorbent material at the TC1 position is carbonated, and the endothermic SMR reaction causes the observed drop in temperature. When the CaO at position TC1 in the reactor is partially to fully carbonated, the temperature at TC2, the position 2.5 cm further down the reactor bed, has started increasing due to CO_2 generation and sorption moving further down the vertical bed. The highest temperature peak, ΔT = 30 °C (690 °C), occurred in the middle of the reactor. This is reasonable as the center part of the reactor is best shielded from heat loss, and heat is transported downstream through convection and conduction. Once the active CaO in the reactor is carbonated, the SMR reaction causes a global decline in temperature (25 min mark). At this point, the set point in the control TC drops below 625 °C, and power is sent to the heating wire. The combination of reactor heating and endothermic SMR/WGS reaction results in rather constant temperature profiles from minute 30 and onward.

The measured temperatures in the second cycle are slightly higher than those of the first cycle. This behavior is expected and can be observed in the CO_2 capacity data reported in Figure 2, where the CO_2 capacity increases from TGA Cycle 1 to TGA Cycle 2. An interesting observation is that the calculated sorption capacity for Cycle 3 is higher than that of Cycle 1, lower than that of Cycle 2, and at the same time exhibits a noticeable decrease in maximum temperature relative to the other two cycles, particularly in the upper portion of the bed (TC1 and TC2). The TC3, TC4, and TC5 peak values for Cycle 3 are comparable to those of the first two cycles. The lower temperature at the bed center during Cycle 3 could be due to the lower temperature upstream, i.e., less energy has been transported down the bed of solids.

Observed temperature is proportional to the rate of CaO carbonation. Given that the initial bed temperature, feed composition, flow, and pressure were the same for all cycles, this temperature profile behavior can be explained by a reduced rate of reaction through a lower CO_2 gas concentration, a lower active mass of CaO (sorbent deactivation), or both. Comparing Figure 4 (*left*) in combination with the carbon balance, one would not immediately expect a significant decrease in peak ΔT values for TC1 and TC2 in Cycle 3 relative to the other two cycles as the CO_2 carrying capacity is retained. A lowered CO_2 concentration in the top part of the solids bed due to slight catalyst migration with maintained catalytic activity is the most plausible explanation for the change in peak temperature for TC1 and TC2 in Cycle 3. The first of two arguments for this explanation is the rise in temperature of TC1 postbreak-through in Figure 4 (*right*) during Cycle 3. At this point, CaO is carbonated, and the temperature decreases before the temperature at the control TC drops below its set point value and the reactor starts providing more heating power. TC1−TC5 profiles are all straight post 30 min for Cycles 1 and 2, and TC3−TC5 are also straight for Cycle 3 after the 30 min mark. However, after the 30 min mark for Cycle 3, TC1 temperature is increasing. This is indicative of reduced SMR activity in the top part of the reactor bed−the same power input at TC1 in Cycle 3 produces a larger rate of temperature increase relative to the first two cycles. Lowered CO_2 generation at the TC1 position in the bed would also explain the 0.2 g CO_2/100 g drop in CO_2 capacity from Cycle 2 to 3 as well as the decrease in dry vol % dry H_2 peak value. Incomplete carbonation at the top portion would decrease the total amount of CO_2 taken up, and a lower rate of CO_2 production would result in lower peak vol % H_2 registered in the effluent. A second argument for catalyst migration was produced when emptying the reactor. Combined particles were intact with negligible traces of orange dust (reduced Cu), while there was a significant amount of black/gray powder alongside the black particles (reduced Ni). A slight catalyst migration without deactivation and a resulting reduced CO_2 production rate at the top portion of the bed explain all observations−SMR

DOI: 10.1021/acs.iecr.9b02372
Ind. Eng. Chem. Res. XXXX, XXX, XXX−XXX

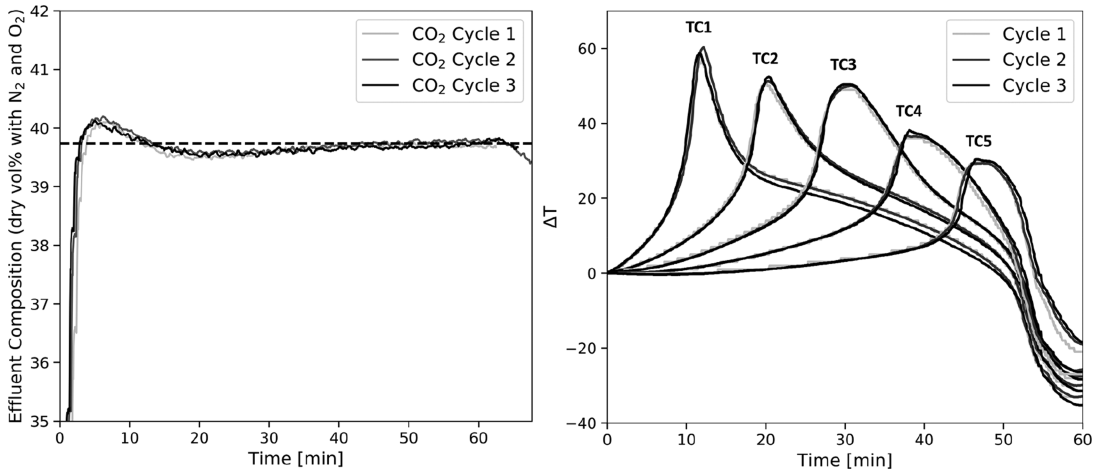

Figure 5. Dry volume percentage measurements (*left*) and thermocouple temperature difference ΔT [°C] (*right*) as functions of time during the Ca−Cu Looping Cu oxidation step for the described combined calcium−copper material. The oxidation was performed at 0.8 MPa, 700−720 °C initial temperature, and diluted air (7.0 vol % O_2). The dashed line (*left*) represents expected CO_2 vol % at full O_2 consumption.

equilibrium composition postbreakthrough, the reduction in peak temperature, the retained CO_2 capture capacity for Cycle 3, and the slightly lowered dry vol % H_2 maximum in Cycle 3 in spite of a higher CO_2 capture capacity than that of Cycle 1.

Overall, the presented material performance is comparable to the performance of segregated materials reported by Díez-Martín et al.[44] for Ca−Cu Looping cycling. The active CaO content is around 12.4 g for both combined and segregated materials tests. There is a difference in peak temperature which is lower in this work (690 °C against 720 °C). This is explained by the $Z < 3.0$ ratio utilized in Díez-Martín et al., the actual $Z = 3.5$ in this work with close to full powder CO_2 capacity being obtained, as well as differences in total flow rates. A decline in observed CO_2 capture capacity is reported in Díez-Martín et al., an expected loss of capacity due to the established 20.0 g CO_2/100 g residual sorbent capacity. It is of note that the combined material has a stable carrying capacity of 14.6−15.0 g CO_2/100 g from the first to the third cycle, in contrast to the declining capacity of the segregated sorbent. Based on the presented data, it seems the CO_2 sorption capacity of the combined materials performs similar to that of segregated sorbent particles under the specified conditions.

Lastly, it can be noted that, though investigations into governing mechanisms for mass transport (be it convective, intra- or interparticle transport) are out of the scope of this experimental validation work, effectiveness factors ranging from 0.3 to 0.8 (depending on reactant and reaction stage) have been implemented in pseudohomogeneous models able to accurately describe the segregated material process in the same experimental rig.[44] These are indications that intraparticle diffusion might play a role for the process depending on the selection of processing conditions. This must be further explored in future work, and if intraparticle diffusion plays a significant role, the intraparticle mass transport properties can be improved by, e.g., optimizing the agglomeration procedure.

3.2.2. Oxidation. Figure 5 depicts measurements of dry volume percent (vol %) composition in the reactor effluent and thermocouple temperatures as functions of time during the Cu oxidation step. The oxidation was performed at 0.8 MPa with initial bed temperatures between 700−720 °C and a 7.0 vol % O_2 gas stream, representing diluted air, 37.0 vol % CO_2, and balance N_2. A plot of temperature profiles in Celsius can be found in the Supporting Information (Figure S2).

During copper oxidation, O_2 (7.0 vol %), N_2 (56.0 vol %), and CO_2 (37.0 vol %) were fed to the reactor. The expected dry flow with full O_2 conversion is 39.75 vol % CO_2. This value is represented by the dotted line in Figure 5 (*left*). Initial signs of material calcination are indicated by an overshoot (5−15 min) of the expected CO_2 vol % value followed by a period of what is interpreted as slow carbonation, indicated by an equal area undershoot (15−40 min). However, the scale of the plotted data should be noted as the overshoot is slight with a 0.44 vol % maximum deviation (Cycle 2), and it can for all practical purposes be considered inconsequential.

A breakthrough of O_2 can indirectly be observed by a drop in CO_2 concentration after 62.5 min on stream for all cycles. By assuming a fully converted 3.6 NL/h flow of O_2 over 62.5 min, a theoretical bed mass of 25.8 g of CuO, or 36.9 wt % CuO, is obtained. This is in good agreement with the 37.6 wt % CuO estimate from powder TGA tests (Table 2). This observation is interesting as it indicates that the oxygen transport properties of the combined material is comparable to that of segregates particles despite being oxidized in the presence of $CaCO_3$ within the same particle.

Based on the thermocouple readings in Figure 5 (*right*), the material oxidation step is reproducible and indicates full oxidation. Like the SER step, the reaction front can be followed by observing the different temperature maxima in time for TC1−TC5. It is of note that the increase in temperature is rather high (ΔT = 65 °C, 771 °C) even with a low flow rate.

The excellent temperature reproducibility of oxidation is an argument for slight catalyst migration rather than combined material deactivation (section 3.2.1). The catalyst effect on oxidation is negligible (1.1 wt % NiO), and thus oxidation is not strongly affected by the presence of catalyst. Previous experience with combined material powders has shown that Cu functionality is more susceptible to loss of capacity and deactivation than the sorbent function.[39] If the copper functionality is retained, it is thus likely that the sorbent function is also retained.

A direct comparison between observed combined material oxygen function versus the segregated material oxygen function

DOI: 10.1021/acs.iecr.9b02372
Ind. Eng. Chem. Res. XXXX, XXX, XXX−XXX

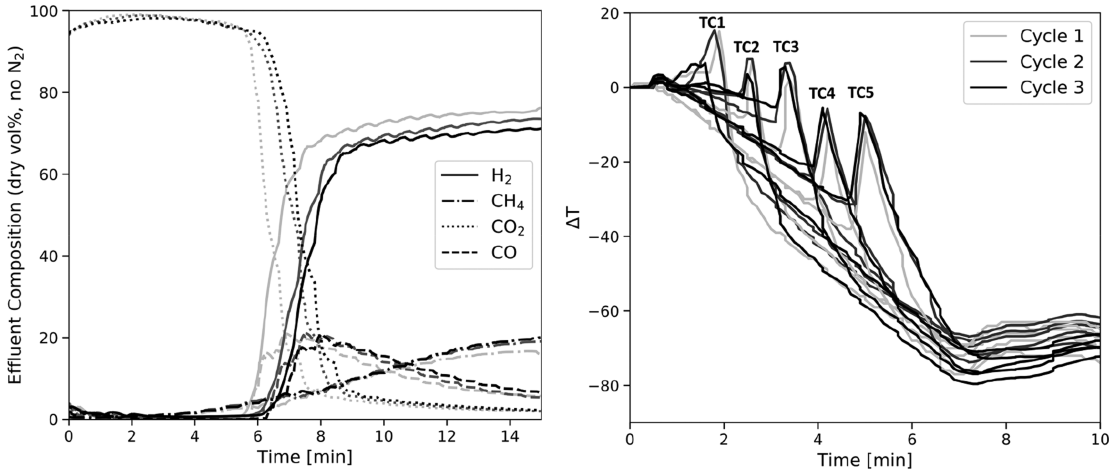

Figure 6. Dry volume percentage measurements (*left*) and thermocouple temperature difference ΔT [°C] (*right*) as functions of time during the Ca−Cu Looping Cu calcination step for the described combined calcium−copper material. The reduction was performed at 0.1 MPa and 800−825 °C initial temperature using 27 vol % CH_4 and 66 vol % H_2 (balance N_2).

reported in Díez-Martín et al. is not feasible due to differences in the reactor copper content and flow rates. However, the oxidation step duration (60−70 min) and the peak temperature (770 °C) are comparable, and the general behavior of the combined material is similar to that of segregated particles.

f6 *3.2.3. Calcination.* Figure 6 depicts measurements of dry volume percent (vol %) composition in the reactor effluent and thermocouple temperatures as functions of time during the calcination step. The calcination was performed at 0.1 MPa with initial bed temperatures between 800 and 825 °C. Prior to sending reducing gases, the reactor set point was changed to 700 °C (effectively stopping reactor heating) in order to minimize effects that could interfere with the calcination temperature profiles. A plot of temperature profiles in Celsius can be found in the Supporting Information (Figure S3).

There is an abrupt change in gas composition once the reducing gas is fed, where close to 100 vol % CO_2 evolves for 3 min. CH_4 slip is detected after 3 min of reduction, possibly due to differences in CuO reduction kinetics with CH_4 and H_2. After 7 min, a slow CH_4 breakthrough is observed along with sharp, simultaneous breakthrough curves of H_2 and CO accompanied by a significant drop in CO_2 concentration. The appearance of CO is interesting as only CH_4 and H_2 are fed through the reactor inlet. CO has been documented in several other works involving calcination.[44,43] The CO concentration has been attributed to SMR/WGS activity and/or CH_4 decomposition. It should be mentioned that CO is a potential product of CH_4 oxidation as well. However, the simplest explanation can be WGS/SMR activity. Initially there are CH_4 and H_2 in the reactor. As $CaCO_3$ calcines and H_2/CH_4 oxidize, there will be significant amounts of CO_2, H_2O, and H_2. The only CO source is CH_4 oxidation, which is evidently relatively slow, as indicated by the observed CH_4 slip. These are conditions for shift toward CO, and both elemental Cu and Ni are present in the reactor during calcination (catalytic activity). The simultaneous breakthrough of H_2 and CO is a result of CuO reduction as H_2 and CO break through once all CuO is reduced. SMR/WGS is in addition able to explain the drop in CO concentration with time: the CO_2 concentration decreases after ended calcination, and there are no sources of H_2O or CO_2 when there is no more CuO for CH_4/H_2 oxidation, causing fed CH_4/H_2 to reach set point values. This effect and the details of CO evolution from the calcination step are fascinating and could be the subjects of a dedicated modeling study.

A carbon balance on the calcination step results in calcination efficiencies of 51−64% for Cycle 1 through Cycle 3. This is in good agreement with the expected 62% calcination efficiency for full carbonation. This observation is consistent with the 14.6−15.0 g CO_2/100 g sorption capacities from the SER step that indicate nearly complete carbonation of the combined material.

Similar to the SER and oxidation steps, a reaction front moves through the bed (Figure 6 (*right*)). A peak temperature due to CuO reduction is closely followed by a marked drop in temperature due to endothermic $CaCO_3$ calcination. The temperature profiles level out after dropping 80 °C. At this point the main portion of calcination is over, the control thermocouple temperature drops below 700 °C, and power input from the reactor heating wire prevents further decline in bed temperature. The temperature profile during calcination is highly reproducible across three cycles, with a similar step duration of 5−6 min in the main portion of the bed. A maximum temperature of 816−820 °C is attained for all cycles.

A 40 wt % CuO loaded combined material prepared using CuO powder has been exposed to three Ca−Cu Looping tests similar to those described here for the $Cu(OH)_2$ prepared combined material in sections 3.2.1−3.2.3 (Supporting Information, Figures S10−S12). The behavior observed for both combined materials is similar, a finding that shows that the obtained results are reproducible for these samples.

f7 **3.3. Characterization of Materials after Reactor Testing.** A diffraction pattern of agglomerates after reactor testing is provided in Figure 7. As expected, the phases identified are CuO, CaO, and $Ca_{12}Al_{14}O_{33}$. Mixed calcium−copper $CaCu_2O_3$ and Ca_2CuO_3 phases observed before cycling segregate into separate CaO and CuO during testing. There is limited information on mixed calcium−copper phases in the literature, but there is evidence suggesting that they are removed by reduction[52] and are retained when no reducing steps are implemented.[53] In the performed Ca−Cu Looping tests, mixed phases seem to disappear after the prereduction and do not form again during testing in reducing conditions. There are no traces of the Ni/Al_2O_3 catalyst. Dust and residue

DOI: 10.1021/acs.iecr.9b02372
Ind. Eng. Chem. Res. XXXX, XXX, XXX−XXX

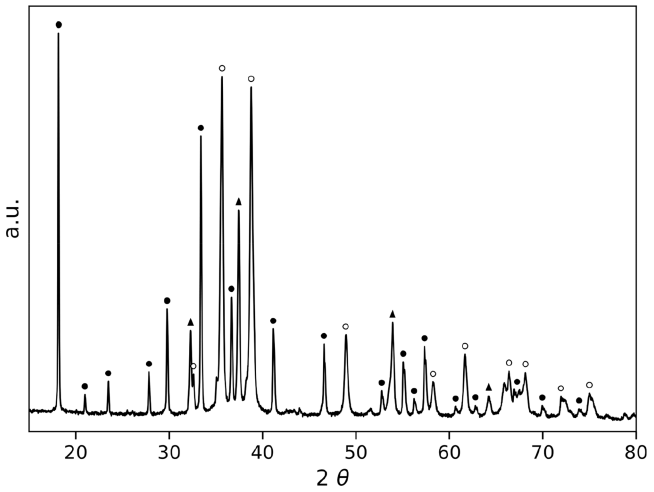

Figure 7. Diffraction pattern for 0.5−0.8 mm combined material agglomerates after reactor testing. All peaks are accounted for and identified as CuO (○), $Ca_{12}Al_{14}O_{33}$ (●), and CaO (▲).

of catalyst material were meticulously removed using a magnet after reactor testing. It is therefore not expected that contamination will obscure the reported characterization results, and it is an indication that potential interaction between the combined material and the catalyst is limited.

Characterization data after reactor testing are summarized in Table 3. Direct comparisons between data presented in Table 2 and Table 3 should be done with caution as the phases are not identical. The particle bulk density is 1.92 after testing and 1.70 prior to reactor testing. The BET area is slightly increased (2.2 to 3.3 $m^2\ g^{-1}$) after the reactor tests, the average pore diameter has decreased (381.4 to 152.7 nm), and the porosity has decreased (53.6 to 47.5%). While all the changes are all relatively small, they indicate that the agglomerates after testing with the CuO, CaO, and $Ca_{12}Al_{14}O_{33}$ phases are slightly denser, with a shift toward lower porosity and smaller average pore size resulting in a net increase in BET surface area. Sintering is in general related to a decrease in surface area. An increase in BET area before and after testing shows that there are no clear signs of sintering.

Table 3. Characterization Data for Agglomerates (0.5−0.8 mm) after Reactor Testing[a]

	agglomerates
surface area [$m^2\ g^{-1}$]	3.32 ± 0.01
true density [g cm^{-3}]	3.66 ± 0.01
average pore diameter [nm]	152.7
porosity	47.5%
particle density [g cm^{-3}]	1.92

[a]True density is based on He pycnometry. Porosity, average pore diameter, and particle density are based on Hg intrusion, while surface area is based on N_2 adsorption (BET).

SEM/EDX results after reactor testing are shown in Figure 8(a)−(e). The agglomerate surface SEM image in Figure 8(a) is comparable to that of Figure 3(a), yet there are visible changes at the particle surface. The copper appears more spherical after testing, it does not seem to be equally well dispersed, and there are indications of cluster formation (center left). This is expected from laboratory testing of powders. The elemental dispersion on a particle level is still homogeneous as can be seen from the cross-sectional EDX mappings in Figure 8(b)−(e). No large copper formations are detected, and the characteristic copper migration to the particle surface previously observed for deactivating combined materials is not evident.

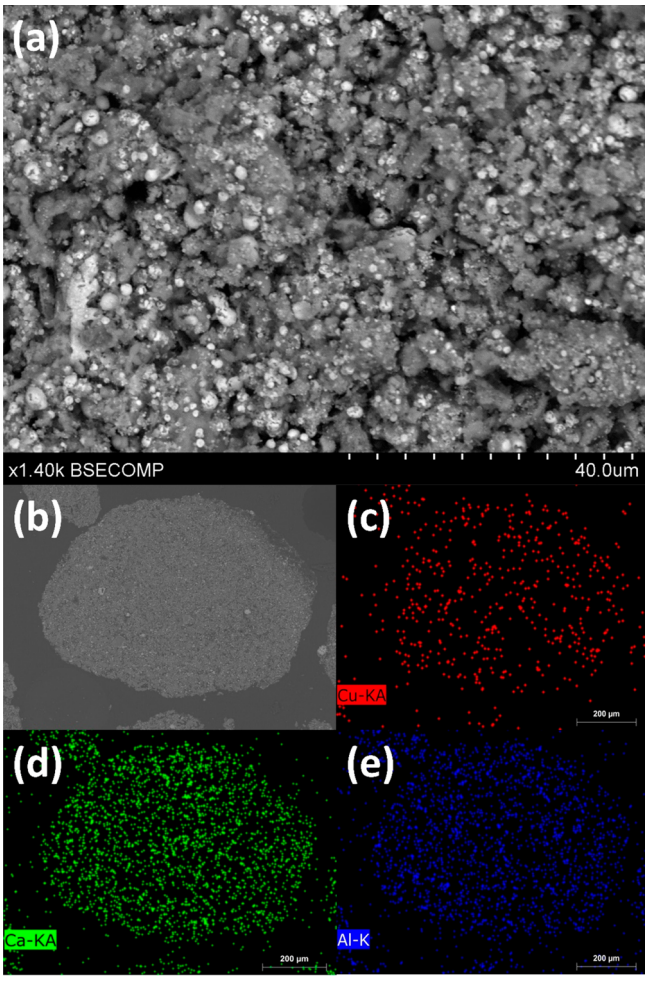

Figure 8. (a) SEM of the agglomerate surface after testing. (b)−(e) Cross-sectional SEM image and EDX mapping of the agglomerate after reactor testing. Cu, Ca, and Al are evenly dispersed throughout the sample. Slight indications of some Cu clustering (light gray) areas in (b) are observed, but no significant migration can be detected.

Characterization of a 40 wt % CuO loaded combined material after testing is provided in the Supporting Information (Figures S4−S9, Tables S1 and S2). The same trends are observed for this material: no mixed calcium−copper phases are identified (CaO, CuO, and $Ca_{12}Al_{14}O_{33}$ only), there is a very slight decrease in porosity and increase in surface area, and there are no pronounced changes in phase dispersion before and after testing.

4. CONCLUSIONS

A mayenite based combined calcium−copper material prepared using $Cu(OH)_2$ as copper(II) oxide precursor has been validated in three full Ca−Cu Looping cycles in a fixed bed reactor. During SER, the combined material was able to capture 14.6−15.0 g CO_2/100 g, reaching peak hydrogen effluent compositions close to those predicted from equilibrium calculations for all cycles (≥98.2% [vol/vol]). The CO_2 capture capacity is in good agreement with the active CaO

DOI: 10.1021/acs.iecr.9b02372
Ind. Eng. Chem. Res. XXXX, XXX, XXX−XXX

content (≥95.4% [wt/wt]) expected from 0.1 MPa TGA tests of combined material powder. The mass transfer resistance observed for the agglomerates in 0.1 TGA tests relative to powder was not observed under the utilized SER conditions—an indication that both the kinetic and diffusion regimes of CaO carbonation were available for reaction. The sorbent carbon capture capacity was stable from the first cycle. This is an advantage with respect to tailoring the combined material CuO/CaO ratio in future work.

The Cu oxidation was complete (36.9 wt % CuO) and in close agreement with 0.1 MPa TGA powder estimates (37.6 wt % CuO). The oxidation of Cu does not seem to be affected by the presence of $CaCO_3$ under the relevant conditions. Calcination was predictable with a 51−64% calcination efficiency for Cycles 1−3, consistent with the CO_2 capture capacity during SER (62% calcination efficiency expected at full carbonation). CO was observed during calcination. This has primarily been attributed to SMR/WGS activity and shift toward CO. Both the reduction and oxidation steps show high degrees of reproducibility throughout the 3 cycles.

Mixed $CaCu_2O_3$ and Ca_2CuO_3 phases are observed for agglomerates before reactor testing. These segregated into CaO, CuO, and $Ca_{12}Al_{14}O_{33}$ during testing. There are minor structural changes in the material before and after testing where the porosity is lowered (53.6 to 47.5%), the surface area is increased (2.2 to 3.3 $m^2\ g^{-1}$), and the average pore diameter is reduced (381.4 to 152.7 nm). There are some signs of Cu migration, as expected from previous work on combined material powders. However, there is still good phase dispersion at the particle level after testing, and the number of Ca−Cu Looping cycles employed is not sufficient for establishing nor rejecting long-term stability of CO_2 and O_2 carrying capacities.

Taken together, the validation of the presented combined material has shown good agreement between laboratory characterization (e.g., TGA, XRD) and actual fixed bed reactor behavior under Ca−Cu Looping conditions. The combined material Cu and CaO functions seem to behave like those of segregated particles. These results are promising for the future development of combined materials. The material concept does indeed appear feasible and can be a viable alternative to a segregated materials approach to Ca−Cu Looping in terms of process intensification given the current state of materials development and larger scale demonstrations.

Ca−Cu Looping has been experimentally validated in a fixed bed containing about 42 wt % of inert in the combined calcium−copper material. To further enhance the calcination efficiency, the amount of CaO has to be decreased from 20 wt % to 14 wt % (active CuO/CaO = 2.8 [wt/wt]). This will result in an increase of the inert fraction in the combined material to 45.6 wt %−given a maintained CuO loading of 40 wt %. For the sake of comparison, in order to achieve the same amount of inert bed fraction per 100.0 g for the segregated materials concept, assuming an oxygen carrier with 60−70 wt % active CuO content,[43,44] an active CaO content in the range 42.9−33.4 wt % (33.6−26.2 g CO_2/100 g stable carrying capacity) is required from the segregated sorbent. When also considering the plausible incremental improvements in CuO loading that can be made in the [40, 50) wt %[39] interval, and that incremental improvement in CuO and CaO loading will greatly reduce the inert fraction in the combined material, the experimental validation carried out in this work shows that combined materials are competitive and the concept is attractive for further studies.

Establishment of long-term transient stability of CO_2/O_2 carrying capacities in a fixed bed reactor through multiple Ca−Cu Looping cycles as well as the CuO/CaO ratio and process optimization are challenges that must be addressed for the combined material in future work. Knowledge gained from the presented validation work combined with reactor modeling can be used for achieving these goals.

■ ASSOCIATED CONTENT

Supporting Information

The Supporting Information is available free of charge on the ACS Publications website at DOI: 10.1021/acs.iecr.9b02372.

Reactor temperature measurements in Celsius for $Cu(OH)_2$ material, characterization results (X-ray diffraction, N_2 adsorption, He pycnometry, Hg intrusion, SEM, EDX), and Ca−Cu Looping reactor results for combined material prepared using CuO powder (PDF)

■ AUTHOR INFORMATION

Corresponding Author

*Phone: +47 992 70 059. E-mail: luca.di.felice@ife.no.

Corresponding author address: Institutt for Energiteknikk (IFE), Instituttveien 18, P.O. Box 40, 2007 Kjeller, Norway.

ORCID

Pascal D. C. Dietzel: 0000-0001-5731-2118

Luca Di Felice: 0000-0002-4378-6408

Notes

The authors declare no competing financial interest.

■ ACKNOWLEDGMENTS

The work is funded by the Research Council of Norway (NFR) within the CLIMIT program − "Innovative Materials for CO_2 Capture by Combined Calcium−Copper Cycles" (project number 254736).

■ REFERENCES

(1) IPCC Working Group III. *IPCC Special Report on Carbon Dioxide Capture and Storage*; Cambridge University Press: United Kingdom and New York, NY, USA, 2005; 442 pp.

(2) Intergovernmental Panel on Climate Change (IPCC). *Global Warming of 1.5 °C*; 2018.

(3) Fennell, P.; Anthony, B. *Calcium and Chemical Looping Technology for Power Generation and Carbon Dioxide Capture*; Woodhead Publishing (Elsevier): Cambridge, UK, 2015.

(4) OECD/IEA. 20 Years of Carbon Capture and Storage - Accelerating Future Deployment. *Carbon Capture*; 2016; 115pp.

(5) IRENA. *Hydrogen from Renewable Power: Technology Outlook for the Energy Transition*; International Renewable Energy Agency: Abu Dhabi, 2018; 52pp.

(6) OECD/IEA. Hydrogen Production & Distribution. *IEA Energy Technology Essentials*; 2007; 4pp.

(7) Riva, L.; Martínez, I.; Martini, M.; Gallucci, F.; van Sint Annaland, M.; Romano, M. C. Techno-Economic Analysis of the Ca-Cu Process Integrated in Hydrogen Plants with CO_2 Capture. *Int. J. Hydrogen Energy* **2018**, *43*, 15720.

(8) Soltani, R.; Rosen, M. A.; Dincer, I. Assessment of CO_2 Capture Options from Various Points in Steam Methane Reforming for Hydrogen Production. *Int. J. Hydrogen Energy* **2014**, *39*, 20266.

(9) Norsk Industri. *Veikart for Prosessindustrien - Økt Verdiskaping Med. Nullutslipp i 2050*; Norsk Industri, Næringslivets Hus: Oslo, Norway, 2019.

(10) DNV GL Energy Markets & Technology. *Produksjon og bruk av hydrogen i Norge*; Synthesis report 2019-0039, Rev. 1; DNV GL: 2019; 134pp.

DOI: 10.1021/acs.iecr.9b02372
Ind. Eng. Chem. Res. XXXX, XXX, XXX−XXX

(11) Höller, S.; Viebahn, P. Assessment of CO_2 Storage Capacity in Geological Formations of Germany and Northern Europe. *Energy Procedia* **2011**, *4*, 4897.
(12) Li, J.; Zhang, H.; Gao, Z.; Fu, J.; Ao, W.; Dai, J. CO_2 Capture with Chemical Looping Combustion of Gaseous Fuels: An Overview. *Energy Fuels* **2017**, *31*, 3475.
(13) Adanez, J.; Abad, A.; Garcia-Labiano, F.; Gayan, P.; de Diego, L. F. Progress in Chemical-Looping Combustion and Reforming Technologies. *Prog. Energy Combust. Sci.* **2012**, *38*, 215.
(14) Lyon, R. K.; Cole, J. A. Unmixed Combustion: An Alternative to Fire. *Combust. Flame* **2000**, *121*, 249−261.
(15) Abanades, J. C.; Murillo, R.; Fernandez, J. R.; Grasa, G.; Martínez, I. New CO_2 Capture Process for Hydrogen Production Combining Ca and Cu Chemical Loops. *Environ. Sci. Technol.* **2010**, *44*, 6901.
(16) Fernández, J. R.; Abanades, J. C.; Murillo, R.; Grasa, G. Conceptual Design of a Hydrogen Production Process from Natural Gas with CO_2 Capture Using a Ca−Cu Chemical Loop. *Int. J. Greenhouse Gas Control* **2012**, *6*, 126.
(17) Fernández, J. R.; Abanades, J. C. Optimized Design and Operation Strategy of a Ca Cu Chemical Looping Process for Hydrogen Production. *Chem. Eng. Sci.* **2017**, *166*, 144.
(18) Martini, M.; Martínez, I.; Gallucci, F.; Romano, M. C.; Chiesa, P.; van Sint Annaland, M. Packed Bed Ca-Cu Looping Process Integrated with a Natural Gas Combined Cycle for Low Emission Power Production. *Energy Procedia* **2017**, *114*, 104.
(19) Ozcan, D. C.; Macchi, A.; Lu, D. Y.; Kierzkowska, A. M.; Ahn, H.; Müller, C. R.; Brandani, S. Ca−Cu Looping Process for CO_2 Capture from a Power Plant and Its Comparison with Ca-Looping, Oxy-Combustion and Amine-Based CO_2 Capture Processes. *Int. J. Greenhouse Gas Control* **2015**, *43*, 198.
(20) Martínez, I.; Armaroli, D.; Gazzani, M.; Romano, M. C. Integration of the Ca−Cu Process in Ammonia Production Plants. *Ind. Eng. Chem. Res.* **2017**, *56*, 2526.
(21) Xu, J.; Froment, G. F. Methane Steam Reforming, Methanation and Water-Gas Shift: I. Intrinsic Kinetics. *AIChE J.* **1989**, *35*, 88.
(22) Živković, L. A.; Pohar, A.; Likozar, B.; Nikačević, N. M. Kinetics and Reactor Modeling for CaO Sorption-Enhanced High-Temperature Water−Gas Shift (SE−WGS) Reaction for Hydrogen Production. *Appl. Energy* **2016**, *178*, 844.
(23) LeValley, T. L.; Richard, A. R.; Fan, M. The Progress in Water Gas Shift and Steam Reforming Hydrogen Production Technologies − A Review. *Int. J. Hydrogen Energy* **2014**, *39*, 16983.
(24) Obradović, A.; Likozar, B.; Levec, J. Steam Methane Reforming over Ni-Based Pellet-Type and $Pt/Ni/Al_2O_3$ Structured Plate-Type Catalyst: Intrinsic Kinetics Study. *Ind. Eng. Chem. Res.* **2013**, *52*, 13597.
(25) Obradović, A.; Likozar, B.; Levec, J. Catalytic Surface Development of Novel Nickel Plate Catalyst with Combined Thermally Annealed Platinum and Alumina Coatings for Steam Methane Reforming. *Int. J. Hydrogen Energy* **2013**, *38*, 1419.
(26) Rostrup-Nielsen, J. R.; Rostrup-Nielsen, T. *Large-Scale Hydrogen Production*; Topsøe Technologies: 2001; 20pp.
(27) Moulijn, J. A.; Makkee, M.; van Diepen, A. *Chemical Process Technology*, 2nd ed.; Wiley: New York, US, 2013; Chapter 5.
(28) Harrison, D. P. Sorption-Enhanced Hydrogen Production: A Review. *Ind. Eng. Chem. Res.* **2008**, *47*, 6486.
(29) Martínez, I.; Romano, M. C.; Chiesa, P.; Grasa, G.; Murillo, R. Hydrogen Production through Sorption Enhanced Steam Reforming of Natural Gas: Thermodynamic Plant Assessment. *Int. J. Hydrogen Energy* **2013**, *38*, 15180.
(30) Baker, E. H. 87. The Calcium Oxide−Carbon Dioxide System in the Pressure Range 1—300 atm. *J. Chem. Soc.* **1962**, *0*, 464.
(31) Martini, M.; van den Berg, A.; Gallucci, F.; van Sint Annaland, M. Investigation of the Process Operability Windows for Ca-Cu Looping for Hydrogen Production with CO_2 Capture. *Chem. Eng. J.* **2016**, *303*, 73.
(32) Alarcón, J. M.; Fernández, J. R. $CaCO_3$ Calcination by the Simultaneous Reduction of CuO in a Ca/Cu Chemical Looping Process. *Chem. Eng. Sci.* **2015**, *137*, 254.
(33) Alarcón, J. M.; Fernández, J. R.; Abanades, J. C. Study of a Cu-CuO Chemical Loop for the Calcination of $CaCO_3$ in a Fixed Bed Reactor. *Chem. Eng. J.* **2017**, *325*, 208.
(34) Qin, C.; Manovic, V.; Ran, J.; Feng, B. Simulation of the Calcination of a Core-in-Shell $CuO/CaCO_3$ Particle for Ca−Cu Chemical Looping. *Fuel* **2016**, *181*, 522.
(35) Manovic, V.; Anthony, E. J. Integration of Calcium and Chemical Looping Combustion Using Composite CaO/CuO-Based Materials. *Environ. Sci. Technol.* **2011**, *45*, 10750.
(36) Manovic, V.; Wu, Y.; He, I.; Anthony, E. J. Core-in-Shell CaO/CuO-Based Composite for CO_2 Capture. *Ind. Eng. Chem. Res.* **2011**, *50*, 12384.
(37) Qin, C.; Yin, J.; Liu, W.; An, H.; Feng, B. Behavior of CaO/CuO Based Composite in a Combined Calcium and Copper Chemical Looping Process. *Ind. Eng. Chem. Res.* **2012**, *51*, 12274−12281.
(38) Kierzkowska, A. M.; Müller, C. R. Sol-Gel-Derived, Calcium-Based, Copper-Functionalised CO_2 Sorbents for an Integrated Chemical Looping Combustion-Calcium Looping CO_2 Capture Process. *ChemPlusChem* **2013**, *78*, 92.
(39) Westbye, A.; Aranda, A.; Dietzel, P. D. C.; Di Felice, L. The Effect of Copper(II) Oxide Loading and Precursor on the Cyclic Stability of Combined Mayenite Based Materials for Calcium Copper Looping Technology. *Int. J. Hydrogen Energy* **2019**, *44*, 12604−12616.
(40) Shokrollahi Yancheshmeh, M.; Radfarnia, H. R.; Iliuta, M. C. High Temperature CO_2 Sorbents and Their Application for Hydrogen Production by Sorption Enhanced Steam Reforming Process. *Chem. Eng. J.* **2016**, *283*, 420.
(41) Díez-Martín, L.; Grasa, G.; Murillo, R.; Martini, M.; Gallucci, F.; van Sint Annaland, M. Determination of the Oxidation Kinetics of High Loaded CuO-Based Materials under Suitable Conditions for the Ca/Cu H 2 Production Process. *Fuel* **2018**, *219*, 76.
(42) Grasa, G.; Navarro, M. V.; López, J. M.; Díez-Martín, L.; Fernández, J. R.; Murillo, R. Validation of the H_2 Production Stage via SER under Relevant Conditions for the Ca/Cu Reforming Process Practical Application. *Chem. Eng. J.* **2017**, *324*, 266.
(43) Fernández, J. R.; Alarcón, J. M.; Abanades, J. C. Study of the Calcination of $CaCO_3$ by Means of a Cu/CuO Chemical Loop Using Methane as Fuel Gas. *Catal. Today* **2019**, *333*, 176−181.
(44) Díez-Martín, L.; López, J. M.; Fernández, J. R.; Martínez, I.; Grasa, G.; Murillo, R. Complete Ca/Cu Cycle for H_2 Production via CH_4 Sorption Enhanced Reforming in a Lab-Scale Fixed Bed Reactor. *Chem. Eng. J.* **2018**, *350*, 1010.
(45) Kazi, S. S.; Aranda, A.; di Felice, L.; Meyer, J.; Murillo, R.; Grasa, G. Development of Cost Effective and High Performance Composite for CO_2 Capture in Ca-Cu Looping Process. *Energy Procedia* **2017**, *114*, 211.
(46) Grasa, G.; Díez-Martín, L.; Murillo, R.; Kazi, S. S.; Aranda, A.; Di Felice, L.; Meyer, J. Experimental Testing of a Bi-Functional Material CaO/CuO Composite with the Ca/Cu H_2 Production Process. *Greenh. Gas Control Techonolgies GHGT-14*; Proceeding Press: 2019.
(47) Westbye, A.; Di Felice, L.; Aranda, A.; Dietzel, P. D. C. Combined Mayenite-Based Calcium-Copper Materials for Ca-Cu Looping Technology: Powder Upscaling and Agglomerate Performance. *Greenh. Gas Control Technologies GHGT-14*; Proceeding Press: 2019.
(48) Navarro, M. V.; López, J. M.; García, T.; Grasa, G.; Murillo, R. Catalyst Evaluation for High-Purity H_2 Production by Sorption-Enhanced Steam-Methane Reforming Coupled to a Ca/Cu Process. *J. Power Sources* **2017**, *363*, 117.
(49) Zamboni, I.; Courson, C.; Kiennemann, A. Fe-Ca Interactions in Fe-Based/CaO Catalyst/Sorbent for CO_2 Sorption and Hydrogen Production from Toluene Steam Reforming. *Appl. Catal., B* **2017**, *203*, 154.

DOI: 10.1021/acs.iecr.9b02372
Ind. Eng. Chem. Res. XXXX, XXX, XXX−XXX

(50) Di Giuliano, A.; Gallucci, K.; Giancaterino, F.; Courson, C.; Foscolo, P. U. Multicycle Sorption Enhanced Steam Methane Reforming with Different Sorbent Regeneration Conditions: Experimental and Modelling Study. *Chem. Eng. J.* **2018**, DOI: 10.1016/j.cej.2018.09.035.
(51) Aloisi, I.; Di Giuliano, A.; Di Carlo, A.; Foscolo, P. U.; Courson, C.; Gallucci, K. Sorption Enhanced Catalytic Steam Methane Reforming: Experimental Data and Simulations Describing the Behaviour of Bi-Functional Particles. *Chem. Eng. J.* **2017**, *314*, 570.
(52) Chen, J.; Duan, L.; Donat, F.; Müller, C. R.; Anthony, E. J.; Fan, M. Self-Activated, Nanostructured Composite for Improved CaL-CLC Technology. *Chem. Eng. J.* **2018**, *351*, 1038.
(53) Duan, L.; Godino, D.; Manovic, V.; Montagnaro, F.; Anthony, E. J. Cyclic Oxygen Release Characteristics of Bifunctional Copper Oxide/Calcium Oxide Composites. *Energy Technol.* **2016**, *4*, 1171.

DOI: 10.1021/acs.iecr.9b02372
Ind. Eng. Chem. Res. XXXX, XXX, XXX−XXX